

Spectroscopic properties of ${}^4\text{He}$ within a multiphonon approach

G. De Gregorio,^{1,2} F. Knapp,³ N. Lo Iudice,⁴ and P. Veselý⁵

¹*Dipartimento di Matematica e Fisica, Università degli Studi della*

Campania "Luigi Vanvitelli", viale Abramo Lincoln 5, I-81100 Caserta, Italy

²*Istituto Nazionale di Fisica Nucleare, Complesso Universitario di Monte S. Angelo, Via Cintia, I-80126 Napoli, Italy*

³*Institute of Particle and Nuclear Physics, Faculty of Mathematics and Physics,
Charles University, V Holešovičkách 2, 180 00 Prague, Czech Republic*

⁴*Dipartimento di Fisica, Università di Napoli Federico II, 80126 Napoli, Italy*

⁵*Nuclear Physics Institute, Czech Academy of Sciences, 250 68 Řež, Czech Republic*

(Dated: February 22, 2022)

Bulk and spectroscopic properties of ${}^4\text{He}$ are studied within an equation of motion phonon method. Such a method generates a basis of n -phonon ($n = 0, 1, 2, 3, \dots$) states composed of tensor products of particle-hole Tamm-Dancoff phonons and then solves the full eigenvalue problem in such a basis. The method does not rely on any approximation and is free of any contamination induced by the center of mass, in virtue of a procedure exploiting the singular value decomposition of rectangular matrices. Two potentials, both derived from the chiral effective field theory, are adopted in a self-consistent calculation performed within a space including up to three phonons. The latter basis states are treated under a simplifying assumption. A comparative analysis with the experimental data points out the different performances of the two potentials. It shows also that the calculation succeeds only partially in the description of the spectroscopic properties and suggests a recipe for further improvements.

I. INTRODUCTION

The studies of few-body nuclear systems have advanced rapidly in the past two decades. The growing computational resources, combined with highly efficient numerical algorithms, have enhanced greatly the performance of traditional methods and stimulated the development of new techniques (see Refs. [1, 2] for review and references).

Most approaches adopt intrinsic coordinates and therefore avoid any interference with the center of mass (c.m.) motion which cannot be averted within standard shell model (SM). The decoupling of the intrinsic from the c.m. motion has been achieved within the no-core SM (NCSM) (see Refs. [3, 4] for a review and references) under the following stringent conditions: (i) Add a c.m. Hamiltonian of frequency ω to the intrinsic one according to the Lawson prescription [5], (ii) use a SM basis built of harmonic oscillator (HO) single particle (s.p.) states of the same frequency, and (iii) include all and only the configurations up to $N_{\text{max}}\hbar\omega$. Being bound to the HO SM basis, the method can be formulated also in terms of Jacobi coordinates [6].

The search for realistic nucleon-nucleon (NN) interactions has evolved in parallel with the search for reliable many body approaches. To this purpose methods for deriving from them effective interactions by softening their repulsive short range components have been developed. Two notable effective potentials are the $V_{\text{low}k}$ [7] obtained by integrating out the high-momentum components of the NN interaction in the free space and the correlated V_{UCOM} obtained through the unitary correlation operator method (UCOM) [8].

It came out that the NN interaction, if used alone, cannot describe the physics of the three-nucleon systems [9].

One needs to introduce the NNN forces. Several semi-phenomenological NNN interactions have been proposed (see Ref. [2] for review and references). A more consistent scheme for their derivation is provided by the chiral effective field theory (χEFT) [10, 11], where the Hamiltonian is generated as a series expansion in terms of the momentum or pion mass. The power counting introduces naturally NN , NNN , and higher order interactions according to a specific hierarchy [12, 13]. The NNN forces appear already at third order (N^2LO). Recently, chiral NN potentials incorporating all contributions from leading order (LO) up to fifth order (N^4LO) have been determined with high accuracy [14, 15]. The χEFT interaction is often smoothed through a similarity renormalization group (SRG) transformation [16] and, so renormalized, is suitable for calculations in truncated shell model spaces, thereby enlarging considerably the domain of applicability of *ab initio* investigations (see Ref. [17] for review and references).

Several *ab initio* approaches, mostly built on NCSM, have adopted the N^2LO or the N^3LO potentials (see Ref. [18] for review and references). Some of them have included the ground-state properties of ${}^4\text{He}$ in the protocol adopted to determine the low-energy constants (LEC) of the χEFT potential [19]. Other realistic calculations have been performed by resorting to the equations of motion method which is known to be an efficient tool for solving the nuclear eigenvalue problem. We mention the coupled cluster (CC) [20] and the in medium SRG (IMSRG) [21], and the random phase approximation (RPA) calculations using UCOM [22] and NNLO_{sat} [23, 24].

A few years ago, we developed for closed shell nuclei an equation of motion phonon method (EMPM) [25–27], which yields an orthonormal multiphonon basis built out of phonons generated in the particle-hole (p-h) Tamm-

Dancoff approximation (TDA) and adopts such a basis to solve the full eigenvalue problem under no approximation apart from the truncation of the multiphonon space. The method was also formulated in the quasiparticle language suitable for open shell nuclei [28] and in the p(h)-phonon scheme for the study of odd-nuclei [29–34].

Very recently, we have endowed the EMPM with a procedure which removes the c.m. spurious admixtures under no constraint and for any s.p. basis [35]. It proceeds in two-steps. We first decouple the c.m. from the TDA states [36] by exploiting the Gram-Schmidt orthogonalization method. We then remove the residual contaminations from the multiphonon basis states by resorting to the singular value decomposition (SVD). This procedure can be easily extended to odd systems and can be adopted within the quasiparticle EMPM to remove at once the contamination induced by the c.m. and the violation of the particle number in open-shell nuclei. In order to show that the method so reformulated can be applied to very light nuclei we have performed an exact calculation using a Hartree-Fock (HF) basis derived from a restricted HO space (up to $N_{max}=5$) for ^4He .

Here we consider a larger HO space in order to offer a more extensive and exhaustive investigation. ^4He was already studied in approaches using Jacobi and hyperspherical coordinates (see for example Refs. [1, 9]) as well as in NCSM [3, 37–40], CC [19, 41], IMSRG [42], and RPA [24]. However, all mentioned studies were focused on its bulk properties or the giant resonance apart from an early NCSM evaluation of the spectrum [43] and a variational approach based on correlated Gaussians which uses the Argonne v8' potential plus a phenomenological three-body force [44].

Ours is a self-consistent approach which covers ground as well as excited states. We adopt two potentials, NNLO_{sat} [19] and Daejeon16 [45], both rooted in the effective field theory. We will refer to them as V_S and V_D , respectively. We will analyze for the two potentials the convergence properties of the ground state (g.s.) observables with respect to the HO frequencies and space dimensions as well as the convergence of two spectra versus the HO frequencies. We also establish an appropriate correspondence between computed and experimental levels by relating their decay mode to the phonon and p-h content of the computed states. Finally, we will investigate the evolution of the electric dipole $E1$ strength distribution as the HO space dimensions increase and show how the redistribution of the $E1$ peaks affects the giant resonance (GR) cross section. We hope that the present investigation may provide some useful insights on the structure of ^4He and some probative indications for more refined tests of the available potentials.

II. BRIEF OUTLINE OF THE METHOD

The basic ingredients are the HF p-h vacuum $|0\rangle$ and the TDA states $|\lambda\rangle = O_\lambda^\dagger |0\rangle$ of energy E_λ , where

$$O_\lambda^\dagger = \sum_{ph} c_{ph}^\lambda (a_p^\dagger \times b_h)^\lambda \quad (1)$$

is the phonon operator built out of the creation and annihilation operators $a_p^\dagger = a_{x_p j_p m_p}^\dagger$ and $b_h = (-)^{j_h+m_h} a_{x_h j_h -m_h}$, which are coupled to spin J_λ and create p-h configurations of energy $\epsilon_p - \epsilon_h$. The λ denotes angular-momentum coupling.

Starting from $|0\rangle$ and the TDA one-phonon states $|\lambda\rangle$, we intend to generate iteratively an orthonormal basis of n -phonon ($n = 2, 3, \dots$) correlated states $|\beta\rangle = |\alpha_n\rangle$ assuming known the $(n-1)$ -phonon basis states $|\alpha\rangle = |\alpha_{n-1}\rangle$ of energy E_α . To this purpose we construct the set of redundant states

$$|(\lambda \times \alpha)^\beta\rangle = \{O_\lambda^\dagger \times |\alpha\rangle\}^\beta \quad (2)$$

and extract from them a basis of linearly independent states by resorting to the Cholesky decomposition method. We are then allowed to write the n -phonon states we search for in the expanded form

$$|\beta\rangle = \sum_{\lambda\alpha} C_{\lambda\alpha}^\beta |(\lambda \times \alpha)^\beta\rangle. \quad (3)$$

They can be determined by solving the generalized eigenvalue equation within the n -phonon subspace

$$\langle(\lambda \times \alpha)^\beta| H |\beta\rangle = E_\beta \langle(\lambda \times \alpha)^\beta|\beta\rangle \quad (4)$$

For our purposes, however, it is more useful to exploit the structure (2) of the states $|(\lambda \times \alpha)^\beta\rangle$ and use the equivalent equation of motion in the reduced form

$$\langle\beta| [H, O_\lambda^\dagger] |\alpha\rangle = (E_\beta - E_\alpha) \langle\beta| O_\lambda^\dagger |\alpha\rangle. \quad (5)$$

Once expanded, the commutator contributes through terms like $\langle\beta| [(a_p^\dagger \times b_h)^{\lambda'} \times (a_r^\dagger \times b_s)^\sigma]^\lambda |\alpha\rangle$, where $(rs) = (pp')$ and $(rs) = (hh')$. We then need just to act on these matrix elements by using the closure

$$I_{n-1} = \sum_\alpha |\alpha\rangle\langle\alpha| \quad (6)$$

and expressing the p-h operators $(a_p^\dagger \times b_h)^{\lambda'}$ in terms of $O_{\lambda'}^\dagger$ upon inversion of Eq. (1).

These operations lead to the generalized eigenvalue equation within the n -phonon subspace

$$\mathcal{H}C = (\mathcal{A}\mathcal{D})C = E\mathcal{D}C, \quad (7)$$

or, more explicitly,

$$\sum_{\lambda'\alpha'} \mathcal{H}_{\lambda\alpha\lambda'\alpha'}^\beta C_{\lambda'\alpha'}^\beta = E_\beta \sum_{\lambda'\alpha'} \mathcal{D}_{\lambda\alpha\lambda'\alpha'}^\beta C_{\lambda'\alpha'}^\beta. \quad (8)$$

Here

$$\mathcal{D}_{\lambda\alpha\lambda'\alpha'}^\beta = \langle (\lambda \times \alpha)^\beta | (\lambda' \times \alpha')^\beta \rangle \quad (9)$$

is the overlap or metric matrix which preserves the Pauli principle and

$$\mathcal{H}_{\lambda\alpha\lambda'\alpha'}^\beta = \sum_{\lambda''\alpha''} \mathcal{A}_{\lambda\alpha\lambda''\alpha''}^\beta \mathcal{D}_{\lambda''\alpha''\lambda'\alpha'}^\beta, \quad (10)$$

where

$$\mathcal{A}_{\lambda\alpha\lambda''\alpha''}^\beta = (E_\lambda + E_\alpha) \delta_{\lambda\lambda''} \delta_{\alpha\alpha''} + \mathcal{V}_{\lambda\alpha\lambda''\alpha''}^\beta. \quad (11)$$

The expressions of the overlap matrix \mathcal{D} and of the phonon-phonon interaction \mathcal{V} can be found, for instance, in Ref. [46]. The solution of Eq. (8) yields the n -phonon basis states (3).

The iteration of the procedure up to an arbitrary n produces a set of states which, added to HF ($|0\rangle$) and TDA ($\{|\alpha_1\rangle\} = \{|\lambda\rangle\}$), form an orthonormal basis $\{|\alpha_n\rangle\}$ ($n = 0, 1, 2, 3, \dots$). Such a basis is then adopted to solve the eigenvalue problem in the full space

$$\sum_{\alpha_n\beta_{n'}} \left((E_{\alpha_n} - \mathcal{E}_\nu) \delta_{\alpha_n\beta_{n'}} + \mathcal{V}_{\alpha_n\beta_{n'}} \right) \mathcal{C}_{\beta_{n'}}^\nu = 0, \quad (12)$$

where $\mathcal{V}_{\alpha_n\beta_{n'}} = 0$ for $n' = n$.

For $n' = n + 1$ ($n > 0$) we have ($\alpha = \alpha_n, \beta = \beta_{n+1}$)

$$\mathcal{V}_{\alpha\beta} = \sum_{\sigma\alpha'} \mathcal{V}_{\alpha\alpha'}^\sigma \langle (\sigma \times \alpha')^\beta | \beta \rangle, \quad (13)$$

where

$$\mathcal{V}_{\alpha\alpha'}^\sigma = \frac{1}{[\alpha]^{1/2}} (-)^{\alpha+\alpha'+\sigma} \sum_{r \leq s} \mathcal{V}_{rs}^\sigma \langle \alpha' || (a_r^\dagger \times b_s)^\sigma || \alpha \rangle \quad (14)$$

and

$$\mathcal{V}_{rs}^\sigma = \sum_{ph} c_{ph}^\sigma F_{rsph}^\sigma. \quad (15)$$

Here

$$F_{rsph}^\sigma = \sum_\gamma (2\gamma + 1) (-)^{r+h-\sigma-\gamma} W(rps h; \gamma \sigma) V_{rps h}^\gamma, \quad (16)$$

where V is the two-body potential and W are Racah coefficients.

The coupling of the vacuum to the two-phonon states is given by

$$\langle 0 | H | \alpha_2 \rangle = \sum_{\lambda\lambda'} \langle (\lambda \times \lambda')^0 | \alpha_2 \rangle \langle \lambda | V | \lambda' \rangle. \quad (17)$$

For $n' = n + 2$ ($n > 0$) the matrix elements can be written in the simple form

$$\mathcal{V}_{\alpha_n\beta_{n'}} = \sum_{\alpha_2} \langle 0 | H | \alpha_2 \rangle \langle (\alpha_2 \times \alpha_n)^\beta | \beta_{n'} \rangle \quad (18)$$

The solution of the final eigenvalue Eq. (12) yields the eigenvectors ($n = 0, 1, 2, 3, \dots$)

$$|\Psi_\nu\rangle = \sum_{n,\alpha_n} \mathcal{C}_{\alpha_n}^\nu |\alpha_n\rangle. \quad (19)$$

III. REMOVAL OF THE C.M. MOTION

The preliminary step [36] consists in adopting Gram-Schmidt to extract from the n_{ph} p-h configurations a set of $n_{ph} - 1$ states orthogonal to

$$|\lambda_{c.m.}, \mu\rangle = \frac{1}{N} R_\mu |0\rangle, \quad (20)$$

where R defines the c.m. coordinates and N is a normalization constant. The states so obtained yield $n_{ph} - 1$ c.m. free TDA phonons.

Let us now consider the two-phonon subspace and separate the n states

$$\{|i\rangle\} = \{ |(\lambda \times \lambda')^\alpha\rangle \}, \quad (21)$$

composed of the c.m. free phonons $|\lambda\rangle$, from the m ones

$$\{|s\rangle\} = \{ |(\lambda \times \lambda_{c.m.})^\alpha\rangle, |(\lambda_{c.m.} \times \lambda_{c.m.})^\alpha\rangle \} \quad (22)$$

containing at least one c.m. phonon $|\lambda_{c.m.}\rangle$. The overlap between the two set of states is non vanishing

$$\mathcal{D}_{si}^{(c.m.)} = \langle s | i \rangle \neq 0 \quad (23)$$

and, therefore, reintroduces the c.m. contamination in the two-phonon states $|\alpha\rangle$.

We need, therefore, to construct a new basis of states

$$|\alpha\rangle = \sum_i C_i^\alpha |i\rangle \quad (24)$$

out of the set of $|i\rangle$, which fulfills the orthogonality condition

$$\langle \alpha | s \rangle = 0 \quad (25)$$

for all $|s\rangle$ c.m. states and any $|\alpha\rangle$. This amounts to determine the right null space of the rectangular matrix $\mathcal{D}^{(c.m.)}$

$$\mathcal{D}^{(c.m.)} C = 0, \quad (26)$$

a goal achieved by a procedure exploiting the SVD.

According to the SVD, the $m \times n$ rectangular matrix $\mathcal{D}^{(c.m.)}$ undergoes the following decomposition

$$\mathcal{D}^{(c.m.)} = U \Sigma V^T = \sum_{i=1,m} \mathbf{u}_i \sigma_i \mathbf{v}_i, \quad (27)$$

where U is a left-singular orthonormal $m \times m$ matrix composed of the row singular vectors \mathbf{u}_i acting on the c.m. states, V^T is the transpose of a right-singular orthonormal $n \times n$ matrix V composed of the column singular vectors \mathbf{v}_i acting on the states composed of c.m. free phonons $|\lambda\rangle$, and Σ is an $m \times n$ rectangular diagonal matrix with m non vanishing singular values $\sigma_i \neq 0$.

It is to be noted that the other $n - m$ singular values vanish, $\sigma_i = 0$ for $i = m + 1, n$. Thus, the right-singular

matrix V decomposes into two submatrices. One is composed of the vectors \mathbf{v}_s ($s = 1, m$) and yields the transformed states

$$|\nu_s\rangle = \sum_{i=1,n} v_{si} |i\rangle \quad (s = 1, m) \quad (28)$$

spanning the c.m. spurious subspace.

The other submatrix, which we denote by \mathbb{V} , is composed of the singular vectors \mathbf{v}_r ($r = m + 1, n$) and generates the $n - m$ transformed states

$$|\nu_r\rangle = \sum_{i=1,n} v_{ri} |i\rangle \quad (r = m + 1, n) \quad (29)$$

orthogonal to the c.m. states $|\nu_s\rangle$

$$\langle \nu_r | \nu_s \rangle = 0. \quad (30)$$

These states form the intrinsic subspace we searched for.

We can then apply the transformation \mathbb{V} to the eigenvalue Eq. (7) obtaining

$$\mathcal{H}'C' = E\mathcal{D}'C', \quad (31)$$

where $C' = \mathbb{V}C$, $\mathcal{D}' = \mathbb{V}\mathcal{D}\mathbb{V}^T$, and $\mathcal{H}' = \mathbb{V}\mathcal{H}\mathbb{V}^T$.

The eigenstates

$$|\alpha_2\rangle = \sum_r (\mathbb{V}C)_r |\nu_r\rangle \quad (32)$$

can be recast in terms of the original basis states $|i\rangle = |(\lambda \times \lambda')^\alpha\rangle$.

We adopt the same procedure for the three-phonon subspace once we identify the c.m. spurious states. These are

$$|s\rangle = \{ |(\lambda_{cm} \times \alpha)^\beta\rangle, |(\lambda \times \alpha_{cm})^\beta\rangle, |(\lambda_{cm} \times \alpha_{cm})^\beta\rangle \}, \quad (33)$$

where $|\alpha_{cm}\rangle$ are just the transformed two-phonon states $|\nu_s\rangle$ ($s = 1, m$) corresponding to the non vanishing singular values $\sigma_s \neq 0$.

IV. NUMERICAL IMPLEMENTATION AND RESULTS

We adopt a Hamiltonian of the form

$$H = T_{int} + V, \quad (34)$$

where T_{int} is the intrinsic kinetic energy and V is either V_S [19] or V_D [45]. V_S is obtained by optimizing simultaneously the two-body and three-body components of the χ EFT potential at N2LO with a cutoff parameter $\Lambda = 450$ MeV. In the present calculation the full three-body force is used to generate the HF basis and is truncated at the normal ordered two-body level in solving the multiphonon eigenvalue problem. V_D is derived from the NN component of the N3LO potential [47] in two steps. The NN potential is first softened by a SRG

method [48] with flow parameter $\lambda = 1.5 \text{ fm}^{-1}$ and then subjected to a phase equivalent transformation which determines an optimal set of parameters of the NN force. The absence of three-body forces reduces considerably the computational effort.

The numerical procedure goes through the following steps: (i) Derive a HF basis from a HO space of dimensions N_{max} and frequency ω ; (ii) use the HF states to create the TDA phonon basis; (iii) generate the n -phonon ($n = 2, 3, \dots$) basis by deriving and solving iteratively the EMPM Eq. (7); and (iv) the basis so constructed is adopted to solve the final eigenvalue problem in the multiphonon space [Eq. (12)].

We have performed already an exact calculation using the full n -phonon basis up to $n = 3$ within a HO space including six major shells ($N_{max}=5$). The results obtained using V_S were presented elsewhere [35].

For the larger spaces ($N_{max} > 5$) considered here, we solve exactly the full eigenvalue problem [Eqs. (7) and (12)] up to two phonons ($n = 2$). An exact treatment for $n > 2$ would be too time-consuming. On the other hand, the three-phonon states are far above the experimental region and affect the low-lying one-phonon and two-phonon states only through their coupling. Therefore, we treat them in the diagonal approximation. Namely, we neglect the phonon-phonon interaction $\mathcal{V}_{\lambda\alpha\lambda'\alpha'}$ in Eq. (11) so that the three-phonon eigenvalues are simply

$$E_{\beta_3} \simeq E_{\alpha_2} + E_\lambda. \quad (35)$$

We truncate the three-phonon subspace by including all the states energies $E_{\alpha_2} + E_\lambda < 100$ MeV to solve the final eigenvalue Eq. (12). Moreover, we keep only the leading order term of the overlap matrix (9) in computing the matrix elements $\mathcal{V}_{\alpha_1\beta_3}$ (Eq. (18)) and $\mathcal{V}_{\alpha_2\beta_3}$ [Eq. (13)] which couple the three-phonon $|\beta_3\rangle$ to the one-phonon $|\alpha_1 = \lambda\rangle$ and two-phonon $|\alpha_2\rangle$ states, respectively.

The diagonal approximation was tested in the restricted $N_{max} = 5$ HO space. The deviations of the approximate energies from the exact ones range from ~ 90 keV to ~ 250 keV for V_D and from ~ 30 keV to ~ 500 keV for V_S . The only exception is represented by the 2_1^- whose energy differs from the exact one by ~ 1 MeV in the case of V_S .

A. Ground state

We have evaluated g.s. energies and proton radii for both potentials and studied their convergence properties with respect to HO frequencies and dimensions, up to $\hbar\omega = 25$ MeV and $N_{max} = 12$, respectively. We used intrinsic operators in order to minimize the effect of the c.m. motion on the HF states, as discussed in Ref. [35].

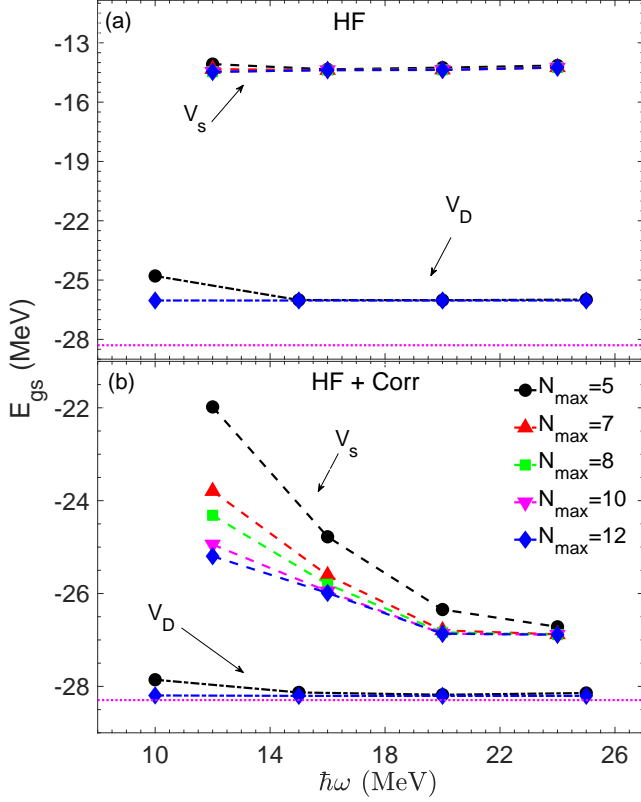


FIG. 1. (Color online) HF and total g.s. energies produced by V_S (dashed lines) and V_D (dot-dashed lines) versus the HO frequency for different dimensions N_{max} . The dotted line indicates the experimental value [49].

1. Energy

The g.s. energy produced by V_S is shared equally between HF and two-phonon correlations (Fig. 1). The HF energy is almost insensitive to the HO frequency (Fig. 1) and reaches a stable value for $N_{max} \geq 7$. The correlation energy, instead, depends appreciably on both frequency and dimensions and reaches convergence for $N_{max} \geq 7$ and $\hbar\omega \geq 20$ MeV. A small gap (~ 1 MeV) with the experiments remains. Most likely, it is due to the residual three-body force, accounted for in creating the HF basis but neglected in the multiphonon calculation. Though determinant in approaching the experimental binding energy, the two-phonon states account only for $\sim 10\%$ of the wave function, which is dominated by HF (Table I).

In the case of V_D , HF accounts almost entirely for energy (Fig. 1) and wave function (Table II). Nonetheless, the binding energy is reproduced just thanks to the small contribution coming from the two-phonon correlations (Fig. 1). The convergence is reached for $\hbar\omega \geq 14$ MeV and $N_{max} \geq 7$.

It is worth mentioning that the g.s. energy is practically insensitive to the c.m. motion whether we use V_S or V_D in perfect agreement with the CC numerical proof that the use of an intrinsic Hamiltonian elimi-

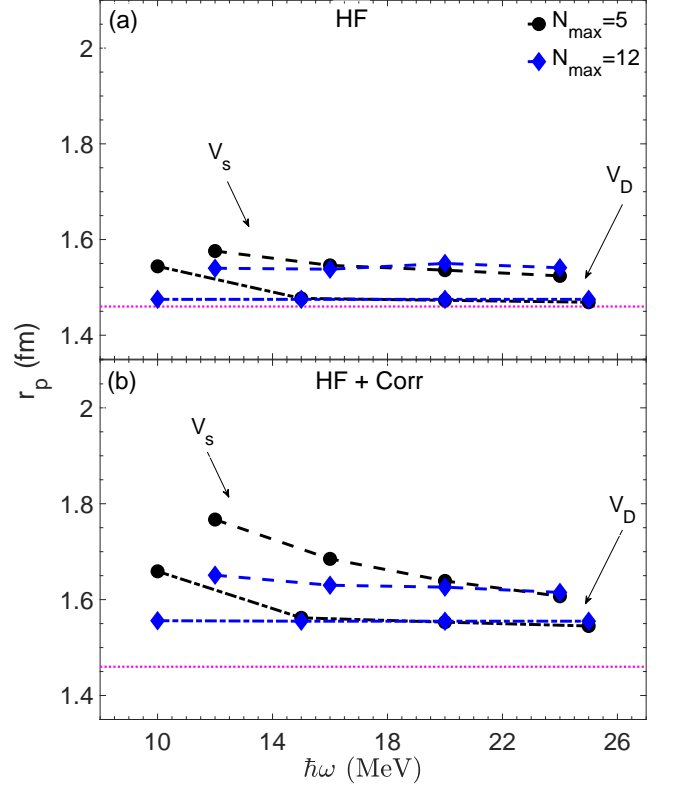


FIG. 2. (Color online) V_S (dashed lines) and V_D (dot-dashed lines) HF and total proton radii r_p versus the HO frequency for different dimensions N_{max} . The dotted line indicates the experimental value [49].

nates almost entirely the c.m. spurious admixtures from the g.s. [51, 52]. For V_S we get $E_{g.s.} = -27.042$ MeV with c.m. admixtures and $E_{g.s.} = -26.866$ MeV without. For V_D we obtain $E_{g.s.} = -28.274$ MeV with c.m. and $E_{g.s.} = -28.205$ MeV without.

2. Proton radius

The proton square radius operator for $N = Z$ is

$$r_p^2 = \frac{1}{Z} \sum_{i=1}^Z (\vec{r}_i - \vec{R}_{cm})^2 = \frac{1}{Z} \left(1 - \frac{1}{A}\right) \sum_{i=1}^Z r_i^2 - \frac{1}{A^2} \sum_{i \neq j=1}^A \vec{r}_i \cdot \vec{r}_j. \quad (36)$$

We have

$$\langle r_p^2 \rangle = \langle \Psi_0 | r_p^2 | \Psi_0 \rangle = \langle r_p^2 \rangle_{HF} + \langle r_p^2 \rangle_{corr}. \quad (37)$$

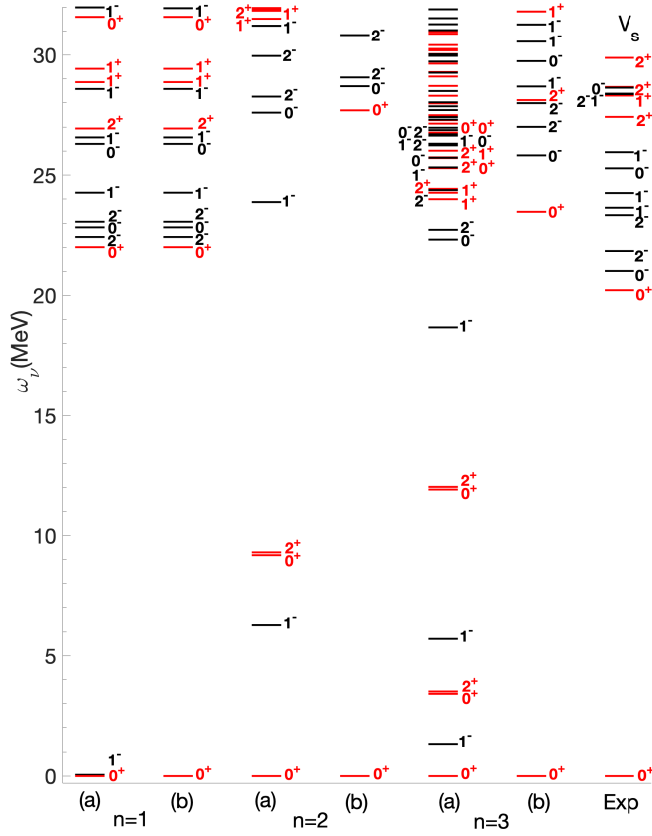


FIG. 3. (Color online) Spectra obtained in different multiphonon spaces before (a) and after (b) having removed the c.m. motion. The calculation was performed using V_S within the restricted $N_{max}=5$ HO space for $\hbar\omega = 20$ MeV. The levels are referred to the HF g.s. ($\omega_\nu = E_\nu - E_{HF}$) in TDA ($n=1$) and to the correlated g.s. ($\omega_\nu = E_\nu - E_0$) for $n=2$ and $n=3$. The experimental data are from Ref. [50].

The first is the HF term, while the second comes from the correlations and is given by

$$\begin{aligned} \langle r_p^2 \rangle_{corr} &= \sum_{\alpha_n \alpha'_n} \mathcal{C}_{\alpha_n}^0 \mathcal{C}_{\alpha'_n}^0 \langle \alpha_n | r_p^2 | \alpha'_n \rangle = \\ &= \sum_{\alpha_2 \alpha'_2} \mathcal{C}_{\alpha_2}^0 \mathcal{C}_{\alpha'_2}^0 \langle \alpha_2 | r_p^2 | \alpha'_2 \rangle, \end{aligned} \quad (38)$$

where use of Eq. (19) has been made and

$$\begin{aligned} \langle \alpha_2 | r_p^2 | \alpha'_2 \rangle &= \frac{1}{Z} \left(1 - \frac{1}{A} \right) \\ &\times \sum_{rs} \langle r \parallel r^2 \parallel s \rangle_p \langle \alpha_2 \parallel (a_r^\dagger \times b_s)^0 \parallel \alpha'_2 \rangle. \end{aligned} \quad (39)$$

It should be pointed out that only the two-phonon subspace contributes and that the two-body term of the square radius originating from the c.m. coordinates (36) vanishes because of the absence of c.m. spurious admixtures in the multiphonon wave function.

The empirical value is extracted from the charge radius

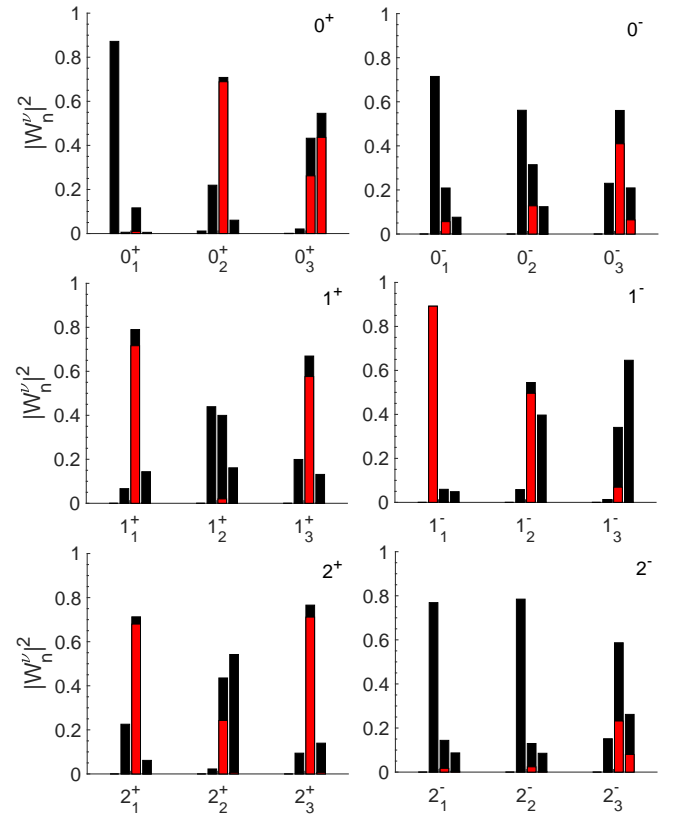


FIG. 4. (Color online) Physical (black) and c.m. spurious (red) content of the different n -phonon components of some typical states before SVD. $W_n^\nu = \sum_{\alpha_n} |\mathcal{C}_{\alpha_n}^\nu|^2$ gives the total weight of the different n -phonon components for a given n [see Eq. (19)]. The bars are ordered from left to right following the sequences $n = 0, 1, 2, 3$ for the 0^+ states and $n = 1, 2, 3$ for the others.

according to the formula [19]

$$\langle r_{ch}^2 \rangle = \langle r_p^2 \rangle + R_p^2 + \frac{N}{Z} R_n^2 + \frac{3\hbar^2}{4m_p^2 c^2}, \quad (40)$$

where $R_p = 0.8775(51)\text{fm}$, $R_n^2 = 0.1149(27)\text{fm}^2$, and $\frac{3\hbar^2}{4m_p^2 c^2} \sim 0.033 \text{ fm}^2$.

As shown in Fig. 2, HF yields almost the whole radius for both potentials. For $N_{max} = 12$, both HF and total radii produced by V_D are insensitive to any frequency. In the restricted $N=5$ HO space, the convergence is reached for $\hbar\omega \geq 15$ MeV. V_S yields a HF radius roughly constant for all frequencies in both HO spaces. The correlations do not alter the convergence properties for $N_{max} = 12$. For $N_{max} = 5$, instead, the convergence is reached slowly for $\hbar\omega \geq 20$ MeV. The radius obtained by V_D almost coincides with the empirical value at the HF level but is shifted slightly upward by the correlations. V_S produces a modest overestimation, incremented slightly by the correlations.

It is interesting to mention the effect induced by the c.m.. Let us consider the more sensitive V_S case. If the

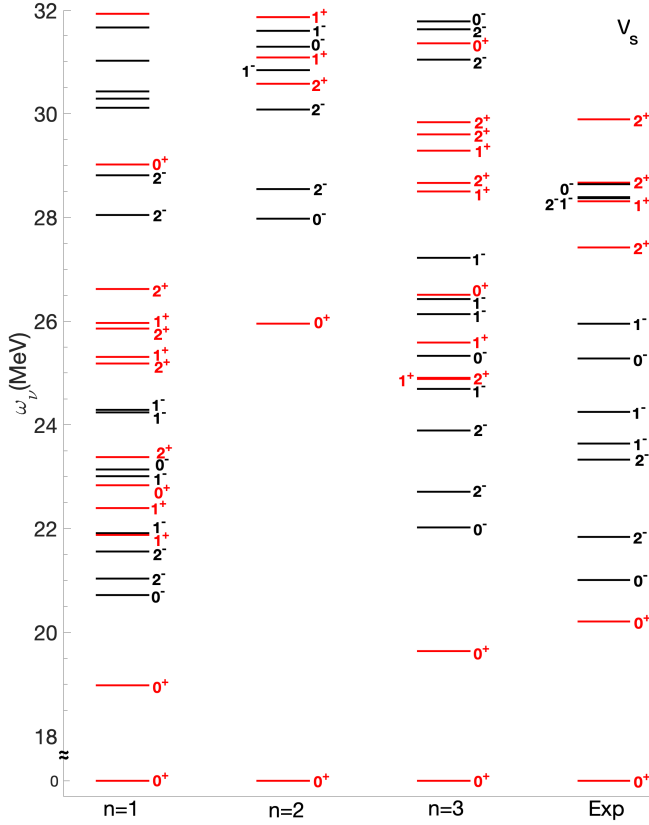


FIG. 5. (Color online) Spectra computed using V_S for $\hbar\omega = 20$ MeV and $N_{max} = 12$ for different multiphonon spaces ($n = 1, 2, 3$). The levels are referred to the HF g.s. ($\omega_\nu = E_\nu - E_{HF}$) in TDA ($n = 1$) and to the correlated g.s. ($\omega_\nu = E_\nu - E_0$) for $n = 2$ and $n = 3$. The experimental data are from Ref. [50].

c.m. is not removed, the non diagonal matrix elements $\langle 0 | \vec{r}_1 \cdot \vec{r}_2 | \alpha_2 \rangle$ are non-vanishing. However, such a contribution is counterbalanced by a comparable enhancement of the two-phonon matrix elements (39). Because of such a mutual cancellation, the radius remains practically unaffected, a further indication that the g.s. observables are insensitive to the c.m. motion.

B. Spectra

1. Impact of the c.m. motion

In order to stress the vital importance of having a c.m. free spectrum, it is sufficient to analyze in more detail the results produced by the exact calculation using V_S within the restricted $N_{max} = 5$ HO space [35]. Figs. 3 and 4 offer a vivid illustration of the dramatic impact of the c.m. motion on the excited states as we move from TDA ($n = 1$) to the multiphonon space. The TDA 1_1^- is practically entirely spurious and is nearly degenerate with the unperturbed HF g.s. state in perfect analogy with

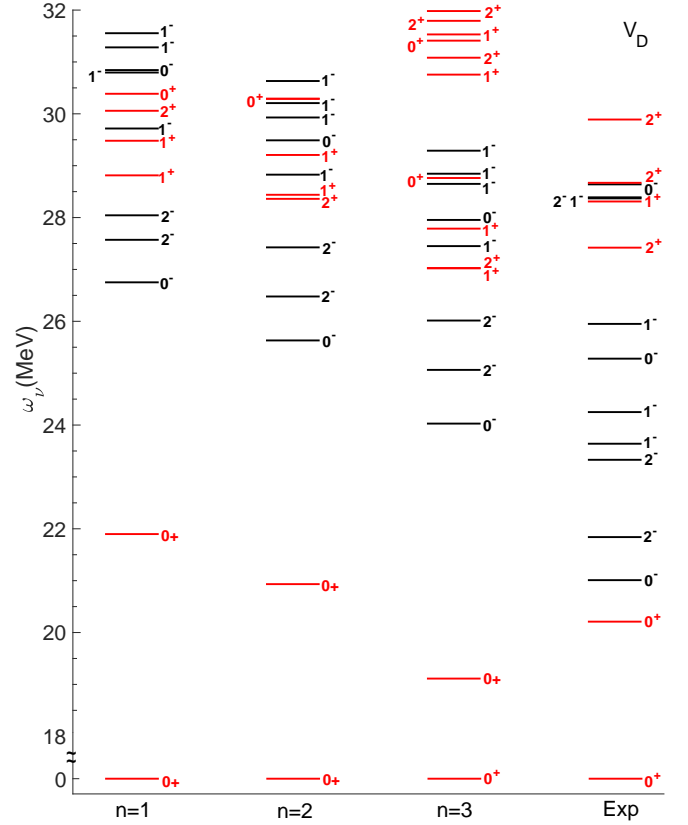


FIG. 6. (Color online) The same as in Fig. 5 for V_D .

RPA. The close similarity between the two approaches, when both adopt a self-consistent single-particle or quasi-particle basis, was discussed in Ref. [36].

The spuriousness propagates among more and more states as the number of phonons increases and distorts dramatically the spectrum as well as the structure of the states. In fact, in addition to the dominantly spurious one-phonon 1_1^- , which gets closer to the correlated g.s., an increasing number of states fall at too low energy. Most of them have two-phonon character and contain one or two spurious TDA 1_1^- phonons (Fig. 4).

It is worth noticing that all these states are not entirely spurious. Their spurious components are admixed with the physical ones of smaller amplitude. Moreover, spurious admixtures are present also in states with dominant c.m. free components. It is therefore impossible to disentangle the physical from the spurious states, hence the crucial role played by the SVD procedure.

2. Convergence properties and comparative analysis

The evolution of the V_S spectrum with the n -phonon subspaces is similar for any HO frequency and dimensions.

Let us consider $N_{max} = 12$ and $\hbar\omega = 20$ MeV (Fig. 5). In perfect analogy with the $N_{max} = 5$ space, the

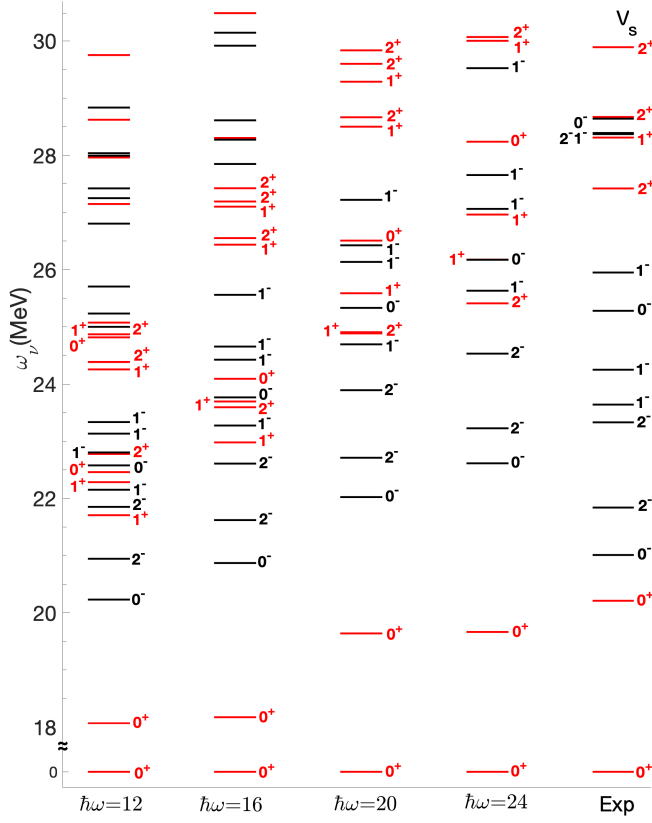


FIG. 7. (Color online) Evolution of the V_S spectrum with the HO frequency. The calculation is performed up to three phonons within a $N_{\max} = 12$ HO space. The experimental data are from Ref. [50].

TDA spectrum falls in the experimental region but is too dense. Moreover, it should be pointed that the levels are referred to the unperturbed HF energy, which is ~ 14 MeV above the experimental value.

The inclusion of the two-phonon subspace produces a large energy gap between excited and ground states and moves most levels above the experimental region. In fact, the coupling of the two phonons to HF [Eq. (17)] is stronger than their coupling to the one-phonon states [Eq. (13)] and therefore induces a strong depression of the g.s. only partly bridged by the downward shift of the excited states.

The coupling of the three phonons to one [Eq. (13)] and two [Eq. (18)] phonons, treated in the diagonal approximation [Eq. (35)], reduces drastically such a distance and brings the whole spectrum back to the experimental region.

The TDA spectrum generated by V_D is quite different (Fig. 6). It is less dense but its levels are at too high energy. Also the evolution with the phonon number is different. No discontinuity is observed in going from one-phonon to two-phonon spaces. Such a smooth behavior was largely expected given the small contribution (~ 2 MeV) to the g.s. energy coming from the correla-

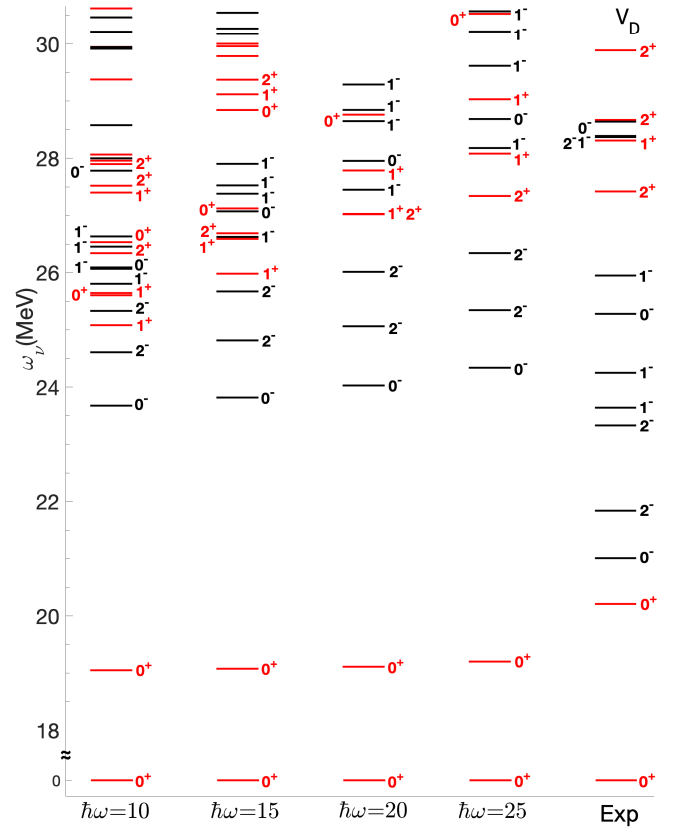


FIG. 8. (Color online) The same as in Fig. 7 for V_D .

tions. On the other hand, because of the minor impact of the multiphonon configurations, the levels get shifted downward smoothly but modestly and, therefore, remain at too high energies.

As shown in Figs. 7 and 8, the trend of the level scheme with the HO frequency is similar for both potentials. It is too compressed and dense for low frequencies, due to the reduced distance between major shells. For $\hbar\omega \geq 20$ MeV, the level density decreases in fair agreement with the experiments. The convergence with the frequency improves but not sufficiently. The differences between the $\hbar\omega = 20$ MeV and the $\hbar\omega = 24$ MeV spectra are not negligible overall and seem to require additional HO shells for a satisfactory convergence, especially for V_S .

For a more detailed comparative analysis, it is appropriate to mention that the lowest seven negative parity states plus the 0_1^- and 1_1^- undergo a nucleon decay while the other levels, all above ~ 27 MeV, undergo a deuteron(D) decay [50]. The first should be put in correspondence with states having a dominant one-phonon component, while the second levels should be associated to states having a dominant two-phonon structure.

From Figs. 5 and 6, we observe for both V_S and V_D spectra a one-to-one correspondence between the first seven theoretical and experimental negative-parity levels. They are, respectively, ~ 1 and ~ 3 MeV above. These states have a dominant one-phonon character (Ta-

TABLE I. Energies and n -phonon composition of the lowest states computed using V_S for $\hbar\omega = 20$ MeV and $N_{\max} = 12$. $W_n^\nu = \sum_{\alpha_n} |C_{\alpha_n}^\nu|^2$ [see Eq. (19)].

J^ν	E^ν	W_0^ν	W_1^ν	W_2^ν	W_3^ν
0_1^+	0.000	0.893	0.007	0.099	0.000
0_2^+	19.639	0.005	0.807	0.114	0.074
0_1^-	22.023	0.000	0.833	0.099	0.068
2_1^-	22.711	0.000	0.843	0.090	0.068
2_2^-	23.892	0.000	0.863	0.066	0.071
1_1^-	24.694	0.000	0.859	0.069	0.071
2_1^+	24.885	0.000	0.832	0.102	0.066
1_1^+	24.907	0.000	0.860	0.068	0.072
0_2^-	25.331	0.000	0.825	0.105	0.070
1_2^+	25.587	0.000	0.867	0.059	0.073
1_2^-	26.135	0.000	0.812	0.122	0.066
1_3^-	26.426	0.000	0.869	0.058	0.073
0_3^+	26.508	0.000	0.878	0.046	0.075
1_4^-	27.220	0.000	0.857	0.072	0.071
1_3^+	28.500	0.000	0.851	0.078	0.071
2_2^+	28.664	0.000	0.869	0.059	0.072
1_4^+	29.286	0.000	0.855	0.073	0.071
2_3^+	29.600	0.000	0.873	0.054	0.073
2_4^+	29.835	0.000	0.840	0.091	0.068
2_6^+	37.780	0.000	0.004	0.970	0.026

bles I and II) and a p-h content roughly compatible with the decay of the corresponding experimental levels (Table III).

Also the lowest 0^+ of both computed spectra has a one-phonon structure and can be related to the experimental 0^+ . However, its p-h content does not match the decay products of the experimental level. It is problematic to identify, among the several theoretical 1^+ levels occurring in both V_S and V_D spectra, the counterpart of the experimental 1^+ .

The theoretical spectra, especially the one generated by V_S , contain additional low-lying positive parity levels plus a 1^- . They have a one-phonon character (Tables I and II) and cannot be associated to the three experimental 2^+ and the $0_3^-, 1_4^-, 2_3^-$ triplet, all undergoing a D decay. The occurrence of these theoretical low-lying positive-parity one-phonon intruders may be traced back to the rather small $(1s, 0d) - (0s)^{-1}$ p-h HF energies which, in turn, generate low TDA levels. We do not have any obvious explanation for the 1^- one-phonon intruder.

The two-phonon states, of both positive and negative parity, which can be associated to the D -decaying levels are at too high energies (~ 38 MeV or above). There are, however, mechanisms for pushing them down. One may consist in enlarging the HO space. Another one is suggested by Eq. (18) which shows that the $(n+2)$ -phonon to n -phonon coupling is proportional to the strong coupling of two phonons to the HF vacuum. We have seen

TABLE II. The same as Table I for V_D .

J^ν	E^ν	W_0^ν	W_1^ν	W_2^ν	W_3^ν
0_1^+	0.000	0.975	0.000	0.024	0.000
0_2^+	19.112	0.001	0.863	0.111	0.026
0_1^-	24.028	0.000	0.862	0.116	0.022
2_1^-	25.063	0.000	0.876	0.106	0.018
2_2^-	26.015	0.000	0.890	0.092	0.018
1_1^+	27.021	0.000	0.890	0.092	0.018
2_1^+	27.027	0.000	0.847	0.136	0.017
1_1^-	27.450	0.000	0.878	0.104	0.018
1_2^+	27.787	0.000	0.896	0.086	0.018
0_2^-	27.954	0.000	0.824	0.152	0.023
1_2^-	28.649	0.000	0.840	0.143	0.017
0_3^+	28.763	0.000	0.888	0.091	0.022
1_3^-	28.845	0.000	0.863	0.119	0.018
1_4^-	29.289	0.000	0.877	0.105	0.018
1_3^+	30.756	0.000	0.865	0.117	0.018
2_2^+	31.082	0.000	0.884	0.099	0.017
0_4^+	31.411	0.000	0.797	0.176	0.027
1_4^+	31.531	0.000	0.872	0.111	0.017
2_3^+	31.793	0.000	0.856	0.127	0.017
2_4^+	31.981	0.000	0.889	0.093	0.017
2_6^+	38.102	0.000	0.006	0.968	0.025

TABLE III. Proton ($\tau = p$) and neutron ($\tau = n$) p-h weights $W_\tau = \sum_{ph} |c_{ph}^\tau|^2$ of the one-phonon (TDA) components of the lowest excited V_S and V_D states compared with the proton ($\%p$) and neutron ($\%n$) decay modes of the experimental levels [53].

J_ν^π	$W_p^{V_S}$	$W_n^{V_S}$	$W_p^{V_D}$	$W_n^{V_D}$	$\%p$	$\%n$
0_2^+	54	46	47	53	100	0
0_1^-	59	41	55	45	76	24
2_1^-	91	9	87	13	63	37
2_2^-	10	90	12	88	53	47
1_1^-	59	41	62	38	55	45
0_2^+	41	59	46	54	52	48
1_2^-	64	36	83	17	50	47
1_3^-	41	59	22	78	52	48
1_1^+	96	4	82	18	48	47

already that such a coupling is responsible for the strong impact of the three phonons on the one-phonon levels. It is therefore natural to expect an analogous effect of the four phonons on the two-phonon states.

In order to obtain a rough estimate of the impact of such a coupling, we make the simplifying assumption that the four-phonon states are composed of two non interacting two-phonon states so that

$$E_{\beta_4} \simeq E_{\beta_2} + E_{\beta_2'} \quad (41)$$

We truncate the subspace by imposing the constraint

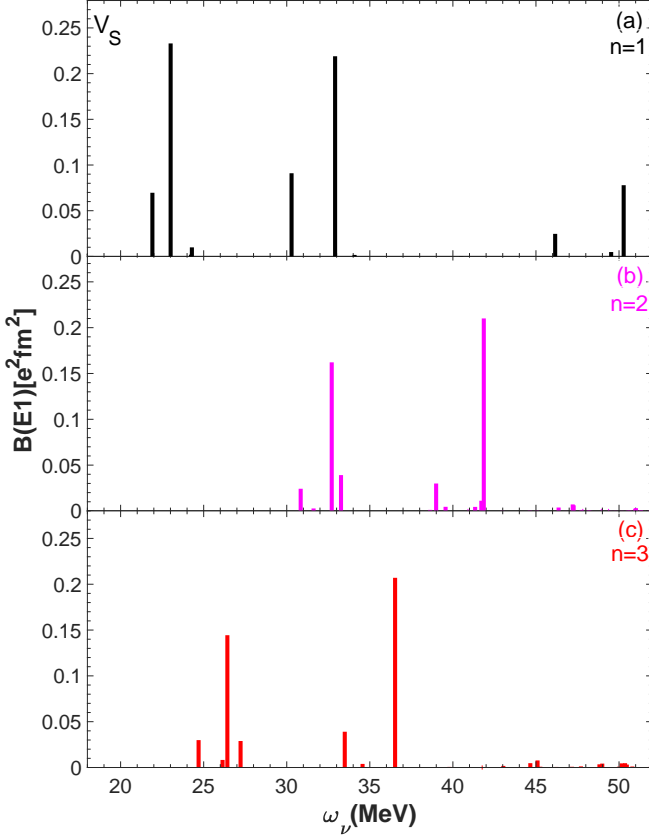


FIG. 9. (Color online) $E1$ spectra computed using V_S and 13 major shells within spaces including up to $n = 1, 2, 3$ phonons.

$E_{\beta_2} + E_{\beta'_2} < 150$ MeV. Furthermore, we compute the coupling [Eq. (18)] by keeping only the leading order term of the overlap matrix $\langle (\alpha_2 \times \alpha'_2)^\beta | \beta_4 \rangle \sim \langle (\alpha_2 \times \alpha'_2)^\beta | (\beta_2 \times \beta'_2)^\beta \rangle \sim \delta_{\alpha_2 \beta_2} \delta_{\alpha'_2 \beta'_2}$.

The two-phonon levels move from ~ 38 to ~ 33 MeV, appreciable but not sufficient to fill the gap with the experiments. We could enlarge the four-phonon subspace for a further shift. For our purpose, however, it is enough to show that the coupling to four phonons is necessary for an exhaustive description of the full spectrum.

C. Dipole transition amplitudes and giant resonance

The absorption electric dipole ($E1$) cross section is given by

$$\begin{aligned} \sigma(E1) &= \int_0^\infty \sigma(E1, \omega) d\omega \\ &= \frac{16\pi^3}{9\hbar c} \int_0^\infty \omega \mathcal{S}(E1, \omega) d\omega, \end{aligned} \quad (42)$$

where $\mathcal{S}(E1, \omega)$ is the strength function

$$\mathcal{S}(E1, \omega) = \sum_\nu B_\nu(E1) \delta(\omega - \omega_\nu). \quad (43)$$

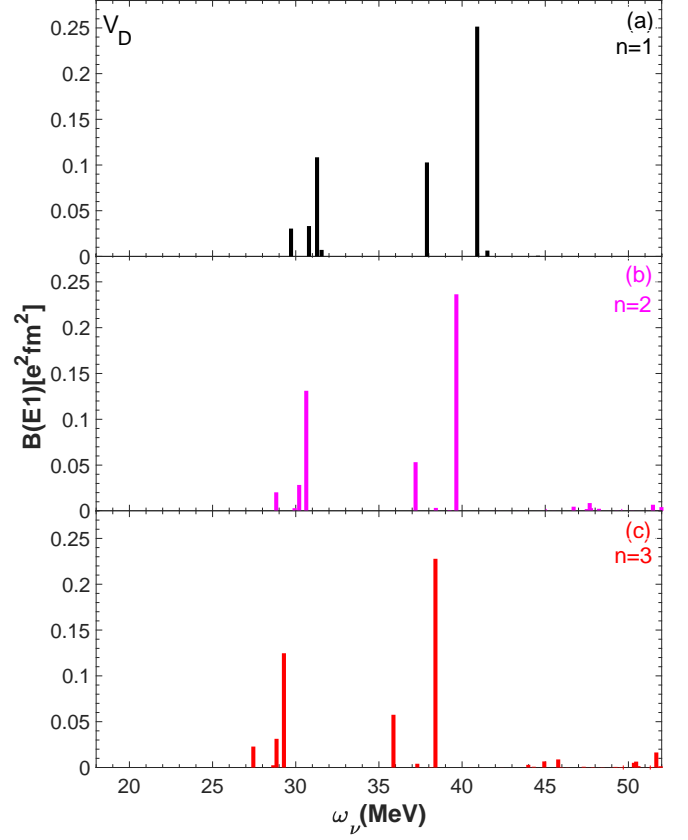


FIG. 10. (Color online) The same as in Fig. 9 for V_D .

The reduced strength

$$B_\nu(E1) = |\langle \Psi_\nu \| \mathcal{M}(E1) \| \Psi_0 \rangle|^2 \quad (44)$$

is determined by the g.s. transition to the ν_{th} final state of energy $\omega_\nu = \mathcal{E}_\nu - \mathcal{E}_0$

$$\begin{aligned} \langle \Psi_\nu \| \mathcal{M}(E1) \| \Psi_0 \rangle &= \\ \sum_{\alpha_n \alpha_{n'}} \mathcal{C}_{\alpha_n}^0 \mathcal{C}_{\alpha_{n'}}^\nu \langle \alpha_{n'} \| \mathcal{M}(E1) \| \alpha_n \rangle, \end{aligned} \quad (45)$$

having made use of Eq. (19) for the wavefunctions.

The electric dipole ($\lambda = 1$) operator has the standard form ($\tau = p, n$)

$$\mathcal{M}(E\lambda\mu) = \frac{1}{[\lambda]^{1/2}} \sum_{(rs)_\tau} e_\tau \langle r \| r^\lambda Y_\lambda \| s \rangle \left[a_r^\dagger \times b_s \right]_\mu^\lambda \quad (46)$$

with proton and neutron bare charges $e_p = e$ and $e_n = 0$.

In the present calculations we replace, as common practice, the δ function appearing in the strength function [Eq. (43)] with a Lorentzian of width Δ .

Our procedure differs from the one adopted in *ab-initio* calculations [58–60] which exploit the Lorentz transform [61] and do not require the explicit determination of all 1^- states as in our case. Thus, position and shape of our cross section depend critically on the positions of the

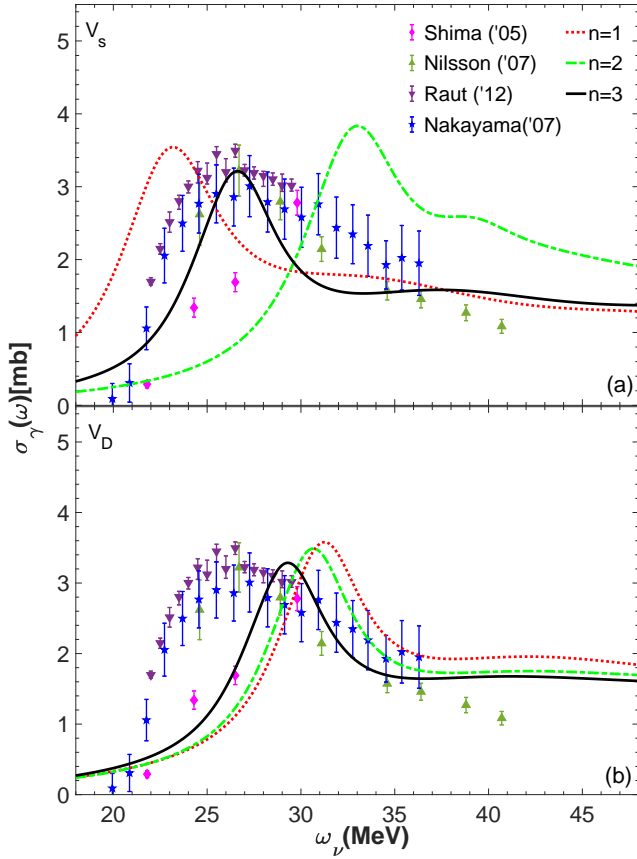


FIG. 11. (Color online) Theoretical GDR cross section computed using V_S (a) and V_D (b) in spaces including up to $n = 1$ (dashed line) $n = 2$ (dotted line), and $n = 3$ (continuous line). The calculation is performed up to three phonons within a $N_{\max} = 12$ HO space for $\hbar\omega = 20$ MeV. The experimental data are taken from Refs. [54–57], assuming, following Ref. [58], $\sigma_\gamma(\omega) \approx 2\sigma_{\gamma,n}(\omega)$ for the data of Ref. [56] and $\sigma_\gamma(\omega) \approx \sigma_{\gamma,p}(\omega) + \sigma_{\gamma,p}(\omega + 0.5 \text{ MeV})$ for those of Ref. [55].

1^- levels and on the distribution of $E1$ strength among them.

The $E1$ g.s. transition strength is ultimately due to the two transitions from the $0s_{1/2}$ to the $0p_{3/2}$ and $0p_{1/2}$ single proton HO states. In HF, the strength spreads over all p-h states containing the $0p_{3/2} - 0s_{1/2}^{-1}$ and $0p_{1/2} - 0s_{1/2}^{-1}$ HO p-h states.

In TDA, the V_S strength gets distributed almost equally among two groups falling in the regions 20-25 and 30-35 MeV (Fig. 9). Both are composed of a short peak and a high peak. The short ones are promoted by the $0s_{1/2} \rightarrow 0p_{3/2}$ transition. The high peaks are due to the $0s_{1/2} \rightarrow 0p_{1/2}$ transition. A residual strength is located in the 45-50 MeV region. An analogous $E1$ spectrum was obtained within a RPA approach using the same potential V_S [24]. The multiphonon states, while fragmenting completely the strength located at 45-50 MeV, cause an overall damping of the other peaks with the exception of the one at ~ 36.5 MeV. However, the two-branch struc-

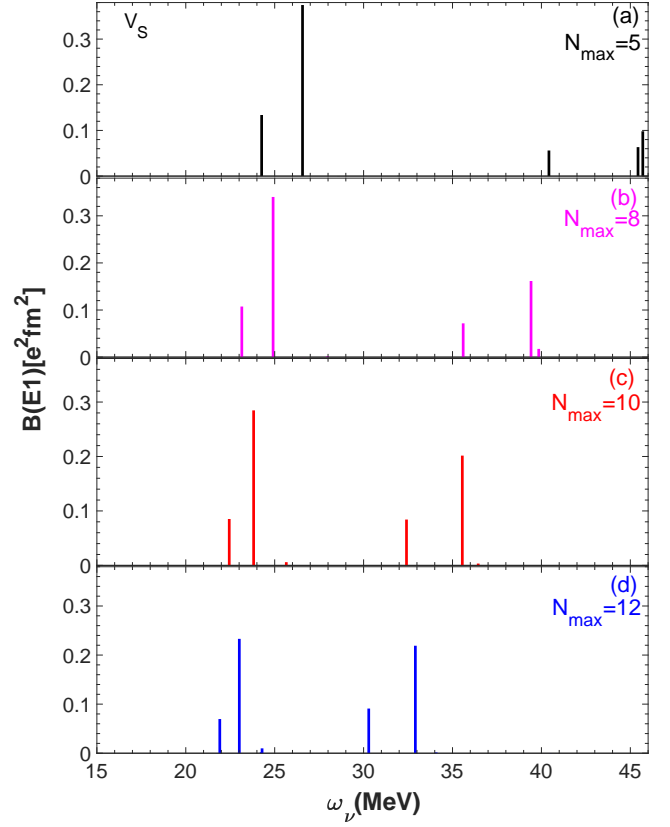


FIG. 12. (Color online) TDA $E1$ spectra computed using V_S versus the HO dimensions N_{\max} for $\hbar\omega = 20$ MeV.

ture persists and the distance between the two groups is unchanged.

The V_D strength splits also into two branches. They are only shifted upward in energy. Such a structure remains unchanged once the two and three phonons are included (Fig. 10).

The two-branch profile persists for both potentials even if we change the frequency. Therefore, it came out to be impossible to try to reproduce the shape of the experimental cross section by using a single width for all levels. The best we have been able to do is to choose two widths. By doing so, we obtain for both potentials a single hump which only roughly approaches the shape of the experimental cross section (Fig. 11).

This result is different from the one obtained in the small space $N_{\max} = 5$, where it was possible to obtain a single hump by using a single width [35]. This difference can be understood if we observe the evolution of the $E1$ strength as the HO dimensions increase. As shown in Fig. 12, for $N_{\max} = 5$, the V_S strength is concentrated almost entirely into two close TDA peaks. The one at ~ 24.3 MeV collects a strength $B(E1) \sim 0.13 e^2 \text{ fm}^2$ and is due mainly to the $0s_{1/2} \rightarrow 0p_{3/2}$ transition. The other at ~ 26.6 MeV is much stronger ($B(E1) \sim 0.37 e^2 \text{ fm}^2$) and arise from the $0s_{1/2} \rightarrow 0p_{1/2}$ transition. A marginal

strength appears at high energy, ~ 45 MeV, and does not interfere with the low-energy hump. The multiphonon states causes only a damping and an upward shift. It was therefore possible to approach the experimental cross section by using a single Lorentzian width $\Delta = 10$ MeV.

However, as N_{max} increases, the high energy peaks move from ~ 45 MeV downward and tend to approach the low-lying branch, whose energy remains almost constant. Moreover, it becomes stronger at the expense of the low-energy transitions. In fact, for $N_{max} = 12$, the TDA strength gets distributed among two doublets of comparable strength. With respect to the small space, the energy separation between them is much smaller but still large (~ 10 MeV). The coupling to three phonons depletes further the low energy peaks in favor of the second ones, but leaves unchanged the separation between the two regions (Fig. 9). Hence the impossibility of getting a one-hump profile by a single width.

The above analysis, however, suggests how to reach our goal. If we enlarge further the HO space, following the trends illustrated in Figs. 9 and 12, the second branch is expected to go down in energy and to collect most of the strength at the expense of the first one, especially once the three-phonon states come into play. Therefore, it should be possible to approach position and shape of the experimental cross section by using a single Lorentzian width. Also the full spectrum should benefit from moving to a larger space.

V. CONCLUSIONS

The different characteristic of the two potentials V_D and V_S have visible effects on the bulk properties of ^4He . V_D privileges HF, which accounts almost entirely for the g.s. energy and proton radius and therefore promotes a fast convergence versus HO frequency and dimensions. Such a fast convergence is due to the softening of the potential induced by SRG. In the case of V_S , instead, HF and two-phonon correlations contribute on equal footing to the energy. Consequently, convergence is reached in a more restricted range of frequencies and sufficiently large dimensions. Such a poor convergence was expected since a bare $NN+NNN$ force was used.

The distinct peculiarities of the two potentials get manifested also in the spectrum. Because of the dominant role played by HF, the level scheme produced by V_D evolves smoothly as we move from the one-phonon to the three-phonon space. The multiphonon states have little impact and do not alter significantly the TDA spectrum. Thus, the resulting levels remain too high with respect to the experimental ones for any HO frequency. In fact, though convergence is not reached, the variations with $\hbar\omega$ are small and tend to enlarge the gap as we increase the frequency. We do not expect a significant improvement even if we enlarge the HO space, given the fast convergence of HF versus N_{max} and the marginal role played by the multiphonon configurations.

In the case of V_S , the multiphonon states play an essential role. The spectrum undergoes dramatic changes in going from $n = 1$ to $n = 2$ and, then, from $n = 2$ to $n = 3$ phonon spaces. Only once the three-phonon states are included, is it possible to establish a satisfactory correspondence between the dominantly one-phonon states and the nucleon decaying levels. No convergence versus the HO frequency is observed. The best proximity to the experiments is obtained for frequencies around $\hbar\omega = 20$ MeV. Given the important role played by the correlations, we should expect further improvements from enlarging the HO space. The dominantly two-phonon states remain at too high energy with respect to the D -decaying levels. However, we have shown that the gap can be drastically reduced by their coupling to four phonons.

The $E1$ V_S and V_D spectra present some analogies but also important differences. In both cases, the strength is distributed mostly among two groups of levels. However, the V_D spectrum is at too high energy and unaffected by the multiphonon configurations. These, instead, are quite effective in the V_S spectrum. In fact, the strength tends to shift from the low to the high energy group of levels as we move from the $n = 1$ to the $n = 3$ space. Another important feature is its sensitivity to the HO space dimensions. The high-energy peaks become more prominent and tend to move down toward the low-lying group of levels as we enlarge the HO space.

This strength redistribution has important impact on the $E1$ giant resonance. Since the two groups of levels are still too far apart for $N_{max} = 12$, we had to use a small and a high Lorentzian width in order to reproduce roughly position and shape of the experimental cross section. We expect that, by enlarging further the HO space, the second dominant group of levels should approach closely the low-lying peaks and, eventually, merge with them. In such a case, a more faithful description of the giant resonance profile should be achieved by enveloping the peaks with a single width. Should this recipe fail, we must conclude that the states constructed out of a bound single-particle basis are not adequate for describing the experimental 1^- excitations lying in the deep continuum. The only remaining alternative would be to resort to the Lorentz transform method.

In summary, the V_D potential has the nice property of privileging HF, thereby promoting a fast convergence versus frequency and dimensions of the HO space. However, it leaves little room for improving the agreement with the experiments through the correlations. These, instead, are essential when V_S is used and, though only for specific frequencies, provide a better description of the spectroscopic properties at the cost of increasing more the dimensions of the HO space. We are confident, however, that even a modest expansion of the space adopted here will promote a significant progress in the description of spectrum and giant resonance.

ACKNOWLEDGMENTS

We thank Petr Navrátil, Mark A. Caprio, Patrick J. Fasano, and Jakub Herko for having provided the matrix elements of the NNLO_{sat} and Daejeon16 potentials. This work was partly supported by the Czech Science Foundation (Czech Republic), P203-19-14048S and by the Charles University Research Center UNCE/SCI/013.

F.K. and P.V. thank the INFN for financial support. Computational resources were provided by the CESNET LM2015042 and the CERIT Scientific Cloud LM2015085, under the program "Projects of Large Research, Development, and Innovations Infrastructures". G. De Gregorio acknowledges the support by the funding program "VALERE" of the Università degli Studi della Campania "Luigi Vanvitelli".

-
- [1] W. Leidemann and G. Orlandini, *Progress in Particle and Nuclear Physics* **68**, 158 (2013).
 - [2] J. Carlson, S. Gandolfi, F. Pederiva, S. C. Pieper, R. Schiavilla, K. E. Schmidt, and R. B. Wiringa, *Rev. Mod. Phys.* **87**, 1067 (2015).
 - [3] P. Navrátil, S. Quaglioni, I. Stetcu, and B. R. Barrett, *Journal of Physics G: Nuclear and Particle Physics* **36**, 083101 (2009).
 - [4] B. R. Barrett, P. Navrátil, and J. P. Vary, *Progress in Particle and Nuclear Physics* **69**, 131 (2013).
 - [5] D. Gloeckner and R. Lawson, *Physics Letters B* **53**, 313 (1974).
 - [6] P. Navrátil and B. R. Barrett, *Phys. Rev. C* **59**, 1906 (1999).
 - [7] A. Nogga, S. K. Bogner, and A. Schwenk, *Phys. Rev. C* **70**, 061002 (2004).
 - [8] H. Feldmeier, T. Neff, R. Roth, and J. Schnack, *Nuclear Physics A* **632**, 61 (1998), ISSN 0375-9474.
 - [9] A. Kievsky, S. Rosati, M. Viviani, L. E. Marcucci, and L. Girlanda, *Journal of Physics G: Nuclear and Particle Physics* **35**, 063101 (2008).
 - [10] S. Weinberg, *Physics Letters B* **251**, 288 (1990).
 - [11] S. Weinberg, *Nuclear Physics B* **363**, 3 (1991).
 - [12] E. Epelbaum, H.-W. Hammer, and U.-G. Meißner, *Rev. Mod. Phys.* **81**, 1773 (2009).
 - [13] R. Machleidt and D. R. Entem, *Physics Reports* **503**, 1 (2011).
 - [14] D. R. Entem, R. Machleidt, and Y. Nosyk, *Phys. Rev. C* **96**, 024004 (2017).
 - [15] P. Reinert, H. Krebs, and E. Epelbaum, *Eur. Phys. J. A* **54**, 86 (2018).
 - [16] S. K. Bogner, R. J. Furnstahl, and R. J. Perry, *Phys. Rev. C* **75**, 061001 (2007).
 - [17] S. R. Stroberg, H. Hergert, S. K. Bogner, and J. D. Holt, *Annual Review of Nuclear and Particle Science* **69**, 307 (2019).
 - [18] P. Navrátil, S. Quaglioni, G. Hupin, C. Romero-Redondo, and A. Calci, *Physica Scripta* **91**, 053002 (2016).
 - [19] A. Ekström, G. R. Jansen, K. A. Wendt, G. Hagen, T. Papenbrock, B. D. Carlsson, C. Forssén, M. Hjorth-Jensen, P. Navrátil, and W. Nazarewicz, *Phys. Rev. C* **91**, 051301 (2015).
 - [20] G. Hagen, T. Papenbrock, M. Hjorth-Jensen, and D. J. Dean, *Reports on Progress in Physics* **77**, 096302 (2014).
 - [21] H. Hergert, *Physica Scripta* **92**, 023002 (2016).
 - [22] N. Paar, P. Papakonstantinou, H. Hergert, and R. Roth, *Phys. Rev. C* **74**, 014318 (2006).
 - [23] N. M. Paruchowski, S. R. Stroberg, P. Navrátil, H. Hergert, and S. K. Bogner, *Phys. Rev. C* **96**, 034324 (2017).
 - [24] Q. Wu, B. S. Hu, F. R. Xu, Y. Z. Ma, S. J. Dai, Z. H. Sun, and G. R. Jansen, *Phys. Rev. C* **97**, 054306 (2018).
 - [25] F. Andreozzi, F. Knapp, N. Lo Iudice, A. Porrino, and J. Kvasil, *Phys. Rev. C* **75**, 044312 (2007).
 - [26] F. Andreozzi, F. Knapp, N. Lo Iudice, A. Porrino, and J. Kvasil, *Phys. Rev. C* **78**, 054308 (2008).
 - [27] D. Bianco, F. Knapp, N. Lo Iudice, F. Andreozzi, and A. Porrino, *Phys. Rev. C* **85**, 014313 (2012).
 - [28] G. De Gregorio, F. Knapp, N. Lo Iudice, and P. Veselý, *Phys. Rev. C* **93**, 044314 (2016).
 - [29] G. De Gregorio, F. Knapp, N. Lo Iudice, and P. Veselý, *Phys. Rev. C* **94**, 061301(R) (2016).
 - [30] G. De Gregorio, F. Knapp, N. Lo Iudice, and P. Veselý, *Phys. Rev. C* **95**, 034327 (2017).
 - [31] G. De Gregorio, F. Knapp, N. Lo Iudice, and P. Veselý, *Phys. Scr.* **92**, 074003 (2017).
 - [32] G. De Gregorio, F. Knapp, N. Lo Iudice, and P. Veselý, *Phys. Rev. C* **97**, 034311 (2018).
 - [33] G. De Gregorio, F. Knapp, N. Lo Iudice, and P. Veselý, *Phys. Rev. C* **99**, 014316 (2019).
 - [34] G. De Gregorio, F. Knapp, N. Lo Iudice, and P. Veselý, *Phys. Rev. C* **101**, 024308 (2020).
 - [35] G. De Gregorio, F. Knapp, N. Lo Iudice, and P. Veselý, *Physics Letters B* **821**, 136636 (2021).
 - [36] D. Bianco, F. Knapp, N. Lo Iudice, P. Veselý, F. Andreozzi, G. De Gregorio, and A. Porrino, *J. Phys. G: Nucl. Part. Phys.* **41**, 025109 (2014).
 - [37] P. Navrátil, *Few Body Syst* **41**, 117 (2007).
 - [38] D. Gazit, S. Quaglioni, and P. Navrátil, *Phys. Rev. Lett.* **103**, 102502 (2009).
 - [39] E. D. Jurgenson, P. Navrátil, and R. J. Furnstahl, *Phys. Rev. Lett.* **103**, 082501 (2009).
 - [40] E. D. Jurgenson, P. Navrátil, and R. J. Furnstahl, *Phys. Rev. C* **83**, 034301 (2011).
 - [41] S. Bacca, N. Barnea, G. Hagen, G. Orlandini, and T. Papenbrock, *Phys. Rev. Lett.* **111**, 122502 (2013).
 - [42] H. Hergert, S. K. Bogner, S. Binder, A. Calci, J. Langhammer, R. Roth, and A. Schwenk, *Phys. Rev. C* **87**, 034307 (2013).
 - [43] D. Zheng and B. Vary, *J.P. and Barrett, Phys. Rev. C* **50**, 2841 (1994).
 - [44] W. Horiuchi and Y. Suzuki, *Few-Body Syst.* **54**, 2407 (2013).
 - [45] A. Shirokov, I. Shin, Y. Kim, M. Sosonkina, P. Maris, and J. Vary, *Physics Letters B* **761**, 87 (2016), ISSN 0370-2693.
 - [46] D. Bianco, F. Knapp, N. Lo Iudice, F. Andreozzi, A. Porrino, and P. Vesely, *Phys. Rev. C* **86**, 044327 (2012).
 - [47] D. R. Entem and R. Machleidt, *Phys. Rev. C* **68**, 041001 (2003).
 - [48] F. Wegner, *Annalen der Physik* **506**, 77 (1994).
 - [49] I. Angeli and K. Marinova, *Atomic Data and Nuclear Data Tables* **99**, 69 (2013), ISSN 0092-640X.

- [50] Data extracted using the NNDC On-line Data Service from the ENSDF database.
- [51] G. Hagen, T. Papenbrock, and D. J. Dean, *Phys. Rev. Lett.* **103**, 062503 (2009).
- [52] G. Hagen, T. Papenbrock, D. J. Dean, and M. Hjorth-Jensen, *Phys. Rev. C* **82**, 034330 (2010).
- [53] D. Tilley, H. Weller, and G. Hale, *Nuclear Physics A* **541**, 1 (1992).
- [54] T. Shima, S. Naito, Y. Nagai, T. Baba, K. Tamura, T. Takahashi, T. Kii, H. Ohgaki, and H. Toyokawa, *Phys. Rev. C* **72**, 044004 (2005).
- [55] B. Nilsson, J.-O. Adler, B.-E. Andersson, J. R. M. Annand, I. Akkurt, M. J. Boland, G. I. Crawford, K. G. Fissum, K. Hansen, P. D. Harty, et al. (The MAX-lab Nuclear Physics Working Group), *Phys. Rev. C* **75**, 014007 (2007).
- [56] R. Raut, W. Tornow, M. W. Ahmed, A. S. Crowell, J. H. Kelley, G. Rusev, S. C. Stave, and A. P. Tonchev, *Phys. Rev. Lett.* **108**, 042502 (2012).
- [57] S. Nakayama, E. Matsumoto, R. Hayami, K. Fushimi, H. Kawasuso, K. Yasuda, T. Yamagata, H. Akimune, H. Ikemizu, M. Fujiwara, et al., *Phys. Rev. C* **76**, 021305 (2007).
- [58] M. D. Schuster, S. Quaglioni, C. W. Johnson, E. D. Jurgenson, and P. Navrátil, *Phys. Rev. C* **92**, 014320 (2015).
- [59] S. Quaglioni and P. Navrátil, *Phys. Lett. B* **652**, 370 (2007).
- [60] S. Bacca, N. Barnea, G. Hagen, M. Miorelli, G. Orlandini, and T. Papenbrock, *Phys. Rev. C* **90**, 064619 (2014).
- [61] V. Efros, W. Leidemann, and G. Orlandini, *Phys. Lett. B* **338**, 130 (1994).